

# Partially Dielectric-Filled Rectangular Waveguide Configuration, Proposed for Broadband and Low Loss Substrate Integrated Waveguides Design

Stefan Simion\*

**Abstract**—In this paper, a new cross section configuration of partially dielectric filled rectangular waveguide (PDF-RW) is proposed and analyzed. It may be used when substrate integrated waveguides (SIWs) are designed such as to maximize the frequency bandwidth for insertion losses as low as possible. Imposing the boundary conditions for the electromagnetic field components, the equations for the cutoff frequencies and propagation constants are developed for the  $TE_{m0}$  modes. It is shown that the cutoff frequency equations developed in this paper may also be used to analyze particular cases investigated by other authors. The ratio between the cutoff frequencies of the  $TE_{20}$  and  $TE_{10}$  modes is computed and represented graphically for different geometric dimensions of the proposed PDF-RW configuration. The conductor and dielectric losses for the  $TE_{10}$  mode are computed as well, based on the results provided by the equations developed in this paper. The results obtained by using the proposed approach are compared to the HFSS (High-Frequency Structure Simulator) results, and very good agreement is observed between them.

## 1. INTRODUCTION

Since the substrate integrated waveguides (SIWs) with rectangular transverse section have been proposed [1–3], the research interest for these transmission media has increased because their losses at high microwave frequencies [4, 5] are lower than the values encountered on transmission lines. Moreover, the technology process for SIWs is fully compatible with the PCB technology commonly used to realize microwave integrated circuits. Assuming that the distance between the metallic via-holes of the SIW is small enough compared to their diameter and the guided wavelength [6, 7], the via-hole arrays approach the electric behavior of the continuous metallic side walls. In this situation, the wave propagation on SIWs may be investigated based on the analysis of the classic rectangular waveguides (RWs), when the boundary conditions may be imposed more easily.

Compared to a hollow RW, the losses in SIW are higher, mainly due to the losses in the solid dielectric. Because of the metallic via-hole arrays used in SIW to model the metallic side walls of the classic RW, it is not possible to remove this dielectric totally, but only partially. In this way, partially dielectric-filled SIWs (PDF-SIW) are obtained [8, 9], and a review of these systems can be found in [10].

Another research direction on SIW is to extend the frequency bandwidth of the dominant mode,  $TE_{10}$ . It can be shown that using via-hole arrays to realize the side walls of the SIWs, only the  $TE_{m0}$  modes may propagate on these types of waveguides [7]. The ratio between the cutoff frequencies of the  $TE_{20}$  and  $TE_{10}$  modes is equal to two for homogeneous RWs [11, 12], but this ratio is different from two for partially dielectric-filled rectangular waveguides (PDF-RWs), as well as for PDF-SIW. If the dielectric slab is located at the center of the PDF-RW between two air regions, it has been

---

Received 13 May 2020, Accepted 27 June 2020, Scheduled 9 July 2020

\* Corresponding author: Stefan Simion (stefan.simion@yahoo.com).

The author is with the Department of Electronics and Communications Engineering, MTA, Bucharest 050141, Romania.

demonstrated analytically that this ratio greater than two is possible [13]. Based on this dielectric configuration, broadband PDF-SIW have been analyzed experimentally in [14, 15], but no theoretical approach or design equations have been proposed. The empty SIW proposed in [8, 9] for reducing the dielectric losses may also be seen as PDF-RW. However, as shown in this paper, the frequency bandwidth for this type of waveguide is less than that for the homogeneous waveguide.

Therefore, a new PDF-RW cross section resulting in a combination of the configurations analyzed in [13] and [8, 9] could be a solution for broadband SIWs with losses as low as possible. In this paper, this new configuration is proposed and analyzed in detail. The  $TE_{m0}$  cutoff frequency equations developed for the proposed PDW-RW may be used to analyze not only the waveguide symmetric configurations proposed in [13–16], but also the homogeneous air-filled or solid dielectric-filled SIWs proposed in [17–19] and [2, 3], respectively.

The paper is organized as follows. In Section 2, the propagation constant and cutoff frequency equations for the  $TE_{m0}$  modes are developed for the proposed PDF-RW. The propagation constants, as well as the ratio between the cutoff frequencies of the  $TE_{20}$  and  $TE_{10}$  modes, are computed and represented graphically for a few geometric dimensions. In Section 3, based on the equations and formulas developed in Section 2, the conductor and dielectric losses for the  $TE_{10}$  mode are computed. The conclusions on the results obtained in Sections 2 and 3 are presented at the end of the paper. Short appendices are given to support the equations developed in this paper.

## 2. $TE_{m0}$ PROPAGATION CONSTANT AND CUTOFF FREQUENCY EQUATIONS

The cross section of the PDF-RW is presented in Fig. 1, where the overall internal RW dimensions are equal to  $a$  and  $b$ , along the  $x$  and  $y$  axes, respectively, while  $\epsilon_{r1}$  and  $\epsilon_{r2}$  are the dielectric constants of the two dielectric materials inside the waveguide metallic walls (usually,  $\epsilon_{r2} = 1$ ). Because of the symmetry with respect to the  $x = 0$  plane, the field analysis may be done between  $x = -a/2$  and  $x = 0$  only, assuming three regions: region 1 is from 0 to  $x = -d/2$ , region 2 from  $x = -d/2$  to  $x = -c/2$ , and region 3 from  $x = -c/2$  to  $x = -a/2$ . The cutoff frequency equations are developed assuming infinite conductivity of the metallic walls and lossless dielectric materials inside the RW.

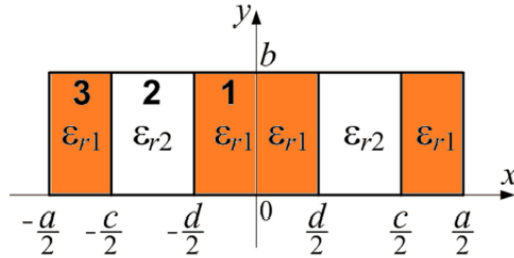


**Figure 1.** The cross section of the PDF-RW analyzed in this paper.

The propagation constant has the same value in all three regions, and it is given by:

$$\beta^2 = k_0^2 \cdot \epsilon_{ri} - k_{ci}^2, \quad i = 1, 2 \text{ and } 3, \quad (1)$$

where  $k_0 = \omega \sqrt{\epsilon_0 \mu_0} = \omega/c_0$  is the propagation constant in free space,  $c_0 = 1/\sqrt{\epsilon_0 \mu_0}$  the speed of the light, and  $k_{ci}$  the cutoff wavenumber in the  $i$ -th region. Since in regions 1 and 3 the dielectric materials are the same, from Eq. (1)  $k_{c1} = k_{c3}$  is obtained.

Assuming time-harmonic dependence, the expressions of the  $TE_{mn}$  axial magnetic field components in the three regions may be written as

$$H_{zi}(x, y, z) = h_{zi}(x, y) \cdot \exp(-j\beta z), \quad (2)$$

where  $h_{zi}(x, y) = X_i(x) \cdot Y_i(y)$ ,  $i = 1, 2$ , and  $3$ , while the expressions for the  $TE_{mn}$  transverse electric field components in the  $i$ -th region are [11, 12]:

$$E_{xi}(x, y, z) = -\frac{j\omega\mu_0}{k_{ci}^2} \cdot \frac{\partial h_{zi}(x, y)}{\partial y} \cdot \exp(-j\beta z) \quad \text{and} \quad (3a)$$

$$E_{yi}(x, y, z) = \frac{j\omega\mu_0}{k_{ci}^2} \cdot \frac{\partial h_{zi}(x, y)}{\partial x} \cdot \exp(-j\beta z), \quad (3b)$$

The functions  $X_i(x)$  and  $Y_i(y)$  in the three regions may be obtained solving the Helmholtz equation  $\Delta_T h_{zi} + k_{ci}^2 h_{zi} = 0$ , by using the method of separation of variables, where  $\Delta_T$  is the Laplace operator in two dimensions. Imposing  $E_{xi} = 0$  at  $y = 0$  and  $y = b$  for any  $x$  and  $z$ , and also the continuity of the electric field components between the three regions,  $Y_i(y) = C$  is obtained for the  $TE_{m0}$  modes. In the following,  $C = 1$  is assumed, hence  $h_{zi}(x, y) = X_i(x)$ ,  $i = 1, 2$ , and 3.

If the  $TE_{m0}$  modes are separated for  $m$  odd and  $m$  even, the expression for the axial transverse magnetic field in the region 1 may be written, as

$$h_{z1}(x) = X_1(x) = \begin{cases} B_1 \sin(k_{c1}x), & \text{for } m \text{ odd} \\ A_1 \cos(k_{c1}x), & \text{for } m \text{ even} \end{cases}, \quad (4a)$$

For the  $TE_{m0}$  mode in region 2, we may write:

$$h_{z2}(x) = X_2(x) = A_2 \cos(k_{c2}x) + B_2 \sin(k_{c2}x), \quad (4b)$$

while imposing  $E_{y3} = 0$  at  $x = \pm a/2$  for any  $y$  and  $z$ , the following expression may be used:

$$h_{z3}(x) = X_3(x) = A_3 \cos \left[ k_{c1} \left( x + \frac{a}{2} \right) \right]. \quad (4c)$$

The boundary conditions for the electric field components among the three regions may be obtained using Eqs. (2), (3b), and (4a)–(4c), imposing  $E_{y1} = E_{y2}$  and  $H_{z1} = H_{z2}$  at  $x = -d/2$ , as well as  $E_{y3} = E_{y2}$  and  $H_{z3} = H_{z2}$  at  $x = -c/2$ , for any  $y$  values from 0 to  $b$ . Combining the resulting expressions, the following equations are obtained (see Appendix A):

$$-\frac{1}{\eta} \cdot \tan \left( k_{c1} \frac{a-c}{2} \right) = \frac{\eta \cdot \tan \left( k_{c1} \frac{d}{2} \right) \cdot \tan \left( k_{c2} \frac{d-c}{2} \right) + 1}{\tan \left( k_{c2} \frac{d-c}{2} \right) - \eta \cdot \tan \left( k_{c1} \frac{d}{2} \right)}, \quad \text{for } m \text{ odd} \quad (5a)$$

and

$$-\frac{1}{\eta} \cdot \tan \left( k_{c1} \frac{a-c}{2} \right) = \frac{\tan \left( k_{c1} \frac{d}{2} \right) - \eta \cdot \tan \left( k_{c2} \frac{d-c}{2} \right)}{\tan \left( k_{c2} \frac{d-c}{2} \right) \cdot \tan \left( k_{c1} \frac{d}{2} \right) + \eta}, \quad \text{for } m \text{ even}, \quad (5b)$$

where  $\eta = k_{c1}/k_{c2}$ .

Taking into account Eq. (1), using the Mathcad software, Equations (5a) and (5b) may be solved for the  $TE_{m0}$  propagation constants  $\beta_{m0}$ . In this way, the normalized waveguide propagation constant  $\beta a$  versus the normalized propagation constant in the free space  $k_0 a$  have been computed for the  $TE_{10}$  and  $TE_{20}$  modes. Numerical results are presented in Fig. 2 (symbols), for  $\varepsilon_{r1} = 4.4$ ,  $\varepsilon_{r2} = 1$  and a few values of the ratios  $c/a$  and  $d/a$ . On the same graphs, the results for homogeneous RWs are also presented, when  $\varepsilon_{r1} = \varepsilon_{r2} = 1$  (the curve for  $c = a$  and  $d = 0$ ) and  $\varepsilon_{r1} = \varepsilon_{r2} = 4.4$  (the curve for  $c = d$ ). The results are compared to those obtained by simulation using HFSS (High-Frequency Structure Simulator [20]) — see the continuous line in Fig. 2. A very good agreement between the results obtained by the two methods is observed.

In particular, if  $\beta_{m0} = 0$ , Equations (5a) and (5b) may be written as follows (in this case, from Eq. (1),  $k_{c1} = k_0 \sqrt{\varepsilon_{r1}}$  and  $k_{c2} = k_0 \sqrt{\varepsilon_{r2}}$ , hence  $\eta = \sqrt{\varepsilon_{r1}/\varepsilon_{r2}}$ ):

$$-\sqrt{\frac{\varepsilon_{r2}}{\varepsilon_{r1}}} \cdot \tan \left[ x \frac{\pi}{2} \sqrt{\varepsilon_{r1}} \left( 1 - \frac{c}{a} \right) \right] = \frac{\sqrt{\frac{\varepsilon_{r1}}{\varepsilon_{r2}}} \cdot \tan \left[ x \frac{\pi}{2} \sqrt{\varepsilon_{r1}} \frac{d}{a} \right] \cdot \tan \left[ x \frac{\pi}{2} \sqrt{\varepsilon_{r2}} \left( \frac{d}{a} - \frac{c}{a} \right) \right] + 1}{\tan \left[ x \frac{\pi}{2} \sqrt{\varepsilon_{r2}} \left( \frac{d}{a} - \frac{c}{a} \right) \right] - \sqrt{\frac{\varepsilon_{r1}}{\varepsilon_{r2}}} \cdot \tan \left[ x \frac{\pi}{2} \sqrt{\varepsilon_{r1}} \frac{d}{a} \right]} \quad \text{for } m \text{ odd}, \quad (6a)$$

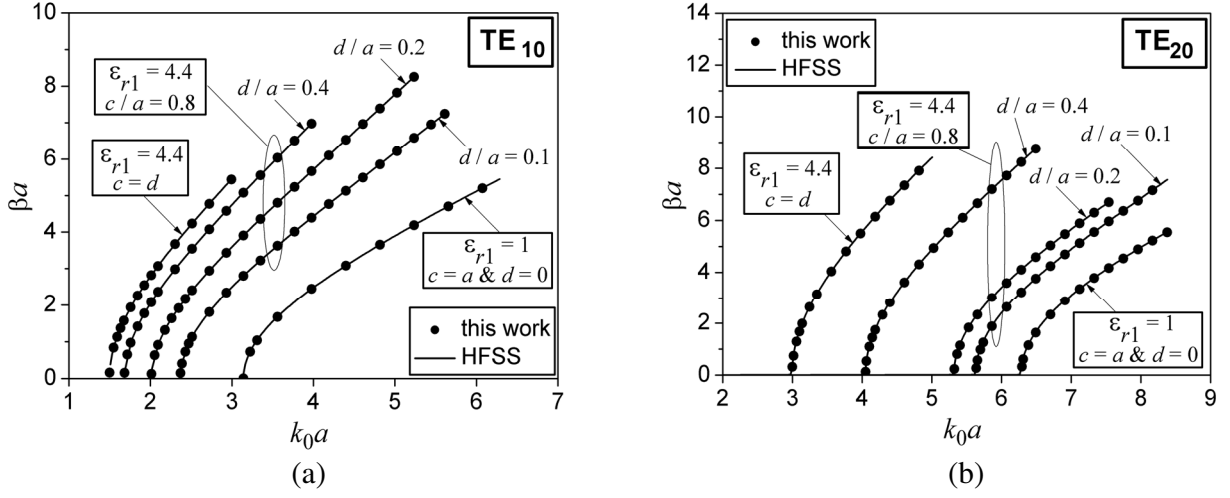


**Figure 2.** The normalized PDF-RW propagation constant  $\beta a$ , versus the normalized free space propagation constant  $k_0 a$ , for the (a)  $TE_{10}$  and (b)  $TE_{20}$  modes and different ratios  $c/a$  and  $d/a$  ( $\epsilon_{r1} = 4.4$  and  $\epsilon_{r2} = 1$ ).

and

$$-\sqrt{\frac{\epsilon_{r2}}{\epsilon_{r1}}} \cdot \tan \left[ x \frac{\pi}{2} \sqrt{\epsilon_{r1}} \left( 1 - \frac{c}{a} \right) \right] = \frac{\tan \left[ x \frac{\pi}{2} \sqrt{\epsilon_{r1}} \frac{d}{a} \right] - \sqrt{\frac{\epsilon_{r1}}{\epsilon_{r2}}} \cdot \tan \left[ x \frac{\pi}{2} \sqrt{\epsilon_{r2}} \left( \frac{d}{a} - \frac{c}{a} \right) \right]}{\tan \left[ x \frac{\pi}{2} \sqrt{\epsilon_{r2}} \left( \frac{d}{a} - \frac{c}{a} \right) \right] \cdot \tan \left[ x \frac{\pi}{2} \sqrt{\epsilon_{r1}} \frac{d}{a} \right] + \sqrt{\frac{\epsilon_{r1}}{\epsilon_{r2}}}} \quad \text{for } m \text{ even,} \quad (6b)$$

where  $x = f_{c\_TE_{m0}}/f_{c\_TE_{10\_air}}$ , while  $f_{c\_TE_{m0}}$  is the  $TE_{m0}$  cutoff frequency, and  $f_{c\_TE_{10\_air}}$  is the  $TE_{10}$  cutoff frequency of the air-filled homogeneous RW. Solving Eqs. (6a) and (6b) for  $x$ , the values for the cutoff frequencies  $f_{c\_TE_{10}}$  and  $f_{c\_TE_{20}}$  may be found. As the ratio  $f_{c\_TE_{20}}/f_{c\_TE_{10}}$  increases, the frequency bandwidth for the propagation of only the  $TE_{10}$  dominant mode increases.

The ratio  $f_{c\_TE_{20}}/f_{c\_TE_{10}}$  versus  $d/a$  has been computed for  $\epsilon_{r2} = 1$  (in region 2 is air), while in regions 1 and 3, three values of the dielectric constant have been assumed,  $\epsilon_{r1} = 2.2$  (RT/duroid 5880), 4.4 (FR4), and 10.2 (RT/duroid 6010). Numerical results are presented in Figs. 3(a) and (b), when

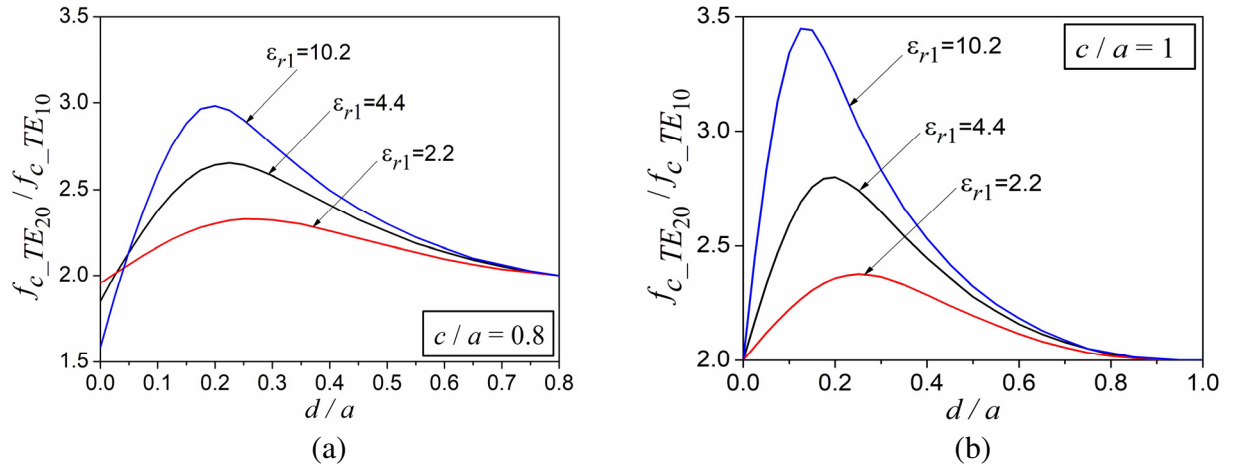


**Figure 3.** The ratio between the cutoff frequencies of the  $TE_{20}$  and  $TE_{10}$  modes versus  $d/a$ , when (a)  $c/a = 0.8$ , and (b)  $c/a = 1$ .

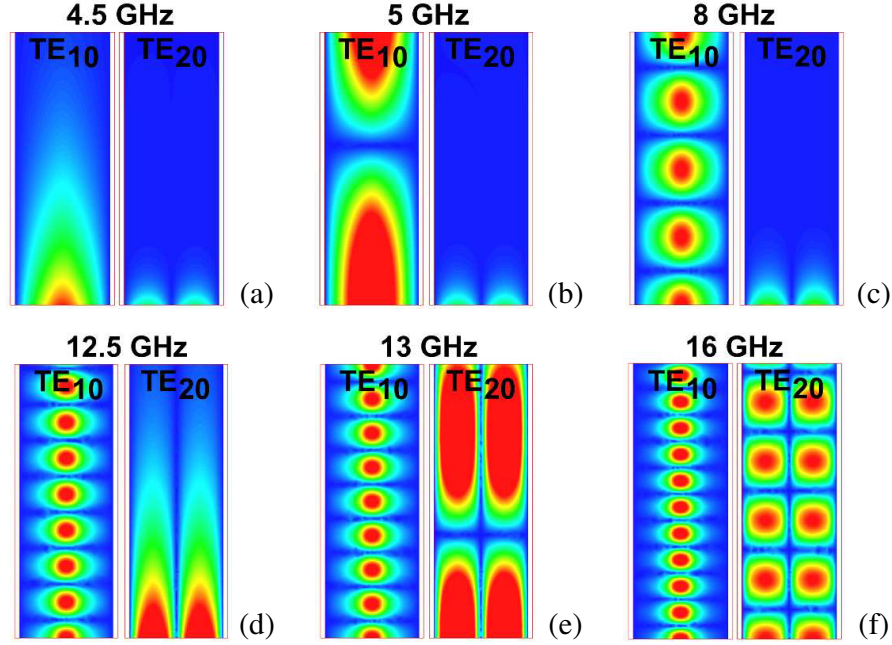


**Figure 4.** HFSS results for the magnitude of the electric field on the PDF-RW broadside wall, along the  $z$ -axis, for  $TE_{10}$  and  $TE_{20}$  waves, when the signal frequency is equal to (a) 4.5 GHz, (b) 5 GHz, (c) 8 GHz, (d) 12.5 GHz, (e) 13 GHz and (f) 16 GHz. The dielectric constant of the solid material which partially fills the PDF-RW is  $\epsilon_{r1} = 4.4$ , while the other dielectric material is air ( $\epsilon_{r2} = 1$ ). Also,  $a = 20$  mm,  $c = 16$  mm,  $d = 4$  mm, the length of the waveguide is equal to 58 mm and  $b = 1.7$  mm (see the cross section shown in Fig. 1).

$c/a$  is equal to 0.8 and 1. For  $c/a = d/a$  (i.e., the homogeneous RW),  $f_{c\_TE20}/f_{c\_TE10} = 2$  is obtained for any value of  $\epsilon_{r1}$ , as expected. From the results presented in the same figures, the peak value of the ratio  $f_{c\_TE20}/f_{c\_TE10}$  increases as the value of  $\epsilon_{r1}$  increases. This peak is as much higher as the ratio  $c/a$  increases. It is observed that there are  $d/a$  values for which  $f_{c\_TE20}/f_{c\_TE10} > 2$  is possible, so that wider frequency bandwidth for propagating of only  $TE_{10}$  mode than the homogeneous RW may be obtained. Also, the numerical results show that  $f_{c\_TE20}/f_{c\_TE10} < 2$  is possible, including for the PDF-RW configuration when  $d = 0$  which has been analyzed in [9] as a solution for low loss SIW. Because of the via-holes fabrication,  $c/a = 1$  cannot be considered in SIW technology, but this case has been analyzed in order to show that the presence of the dielectric material located between  $|x| = c/2$  and  $|x| = a/2$  decreases the frequency bandwidth for the propagation of only the  $TE_{10}$  mode.

If  $a = 20$  mm,  $c = 16$  mm,  $d = 4$  mm,  $\epsilon_{r1} = 4.4$  and  $\epsilon_{r2} = 1$ , the cutoff frequencies values for  $TE_{10}$  and  $TE_{20}$  modes are  $f_{c\_TE10} \cong 4.8$  GHz and  $f_{c\_TE20} \cong 12.7$  GHz. For these geometric and material parameters,  $f_{c\_TE20}/f_{c\_TE10} \cong 2.64$  — see Fig. 3(a). For this particular case, the PDF-RW has been analyzed with HFSS. The simulation results for the magnitude of the  $TE_{10}$  and  $TE_{20}$  electric field on the broadside wall, along the  $z$ -axis, are presented in Fig. 4, for a few signal frequencies. From this figure, the  $TE_{10}$  mode propagates starting from a frequency between 4.5 GHz and 5 GHz, while the  $TE_{20}$  mode propagates starting from a frequency between 12.5 GHz and 13 GHz. These results are in good agreement with the computed values for the cutoff frequencies of the two modes.

Equations (6a) and (6b) may also be used to analyze waveguide configurations already reported by other authors, as shown in the following.

When  $c = a$  (see Fig. 5(a)), Equations (6a) and (6b) may be written as:

$$\sqrt{\frac{\epsilon_{r1}}{\epsilon_{r2}}} \cdot \tan \left[ x \frac{\pi}{2} \sqrt{\epsilon_{r2}} \left( \frac{d}{a} - 1 \right) \right] = -\cot \left[ x \frac{\pi}{2} \sqrt{\epsilon_{r1}} \frac{d}{a} \right], \quad \text{for } m \text{ odd} \quad (7a)$$

and

$$\sqrt{\frac{\varepsilon_{r1}}{\varepsilon_{r2}}} \cdot \tan \left[ x \frac{\pi}{2} \sqrt{\varepsilon_{r2}} \left( \frac{d}{a} - 1 \right) \right] = \tan \left[ x \frac{\pi}{2} \sqrt{\varepsilon_{r1}} \frac{d}{a} \right], \quad \text{for } m \text{ even.} \quad (7b)$$

Equations (7a) and (7b) are the same as reported in [13], where this particular case has been analyzed.

Moreover, if  $d = a$  in Eqs. (7a) and (7b), the homogeneous RW loaded with dielectric material of dielectric constant  $\varepsilon_{r1}$  is obtained (see Fig. 5(b)). In this case, from Eqs. (7a) and (7b),  $x \frac{\pi}{2} \sqrt{\varepsilon_{r1}} = m \frac{\pi}{2}$  is obtained for any  $m$ . Then,  $x = m/\sqrt{\varepsilon_{r1}}$ , or  $f_{c\_TE_{m0}} = m \cdot f_{c\_TE_{10}}/\sqrt{\varepsilon_{r1}}$  for any integer number  $m$ , a result which is well known [11, 12].

Also, the particular case of homogeneous RW loaded with dielectric material of dielectric constant  $\varepsilon_{r2}$  may be obtained if  $c = a$  and  $d = 0$  in Eqs. (6a) and (6b), obtaining  $f_{c\_TE_{m0}} = m \cdot f_{c\_TE_{10}}/\sqrt{\varepsilon_{r2}}$ , as expected.

Another possible particular case is obtained for  $d = 0$ , when the RW cross section is as depicted in Fig. 5(c). In this situation, Equations (6a) and (6b) have the following forms:

$$\sqrt{\frac{\varepsilon_{r2}}{\varepsilon_{r1}}} \cdot \tan \left[ x \frac{\pi}{2} \sqrt{\varepsilon_{r1}} \left( 1 - \frac{c}{a} \right) \right] = \cot \left( x \frac{\pi}{2} \sqrt{\varepsilon_{r2}} \frac{c}{a} \right), \quad \text{for } m \text{ odd} \quad (8a)$$

and

$$\sqrt{\frac{\varepsilon_{r2}}{\varepsilon_{r1}}} \cdot \tan \left[ x \frac{\pi}{2} \sqrt{\varepsilon_{r1}} \left( 1 - \frac{c}{a} \right) \right] = -\tan \left( x \frac{\pi}{2} \sqrt{\varepsilon_{r2}} \frac{c}{a} \right), \quad \text{for } m \text{ even.} \quad (8b)$$

The cutoff frequencies in Equations (8a) and (8b) are the same as reported in [9] for this particular case.

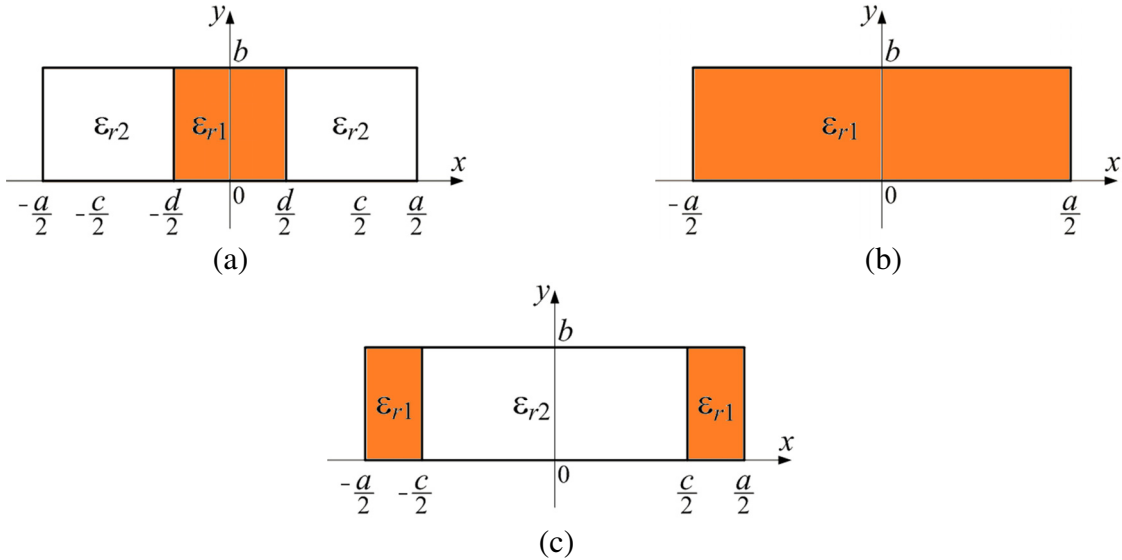


**Figure 5.** Particular configurations of the cross section shown in Fig. 1 which may be also analyzed based on the equations developed in this paper.

### 3. CONDUCTOR LOSSES AND DIELECTRIC LOSSES

The  $TE_{10}$  attenuation constant of the PDF-RW, due to the finite conductivity of the waveguide metallic walls and due to the dielectric losses may be computed with formulas [11, 12]:

$$\alpha_c = P_l/(2P_{10}), \quad (9a)$$

and

$$\alpha_d = P_d/(2P_{10}) \quad (9b)$$

respectively, where

$$P_l = 2R_s \cdot \left[ \int_{-d/2}^0 (|H_{x1}|^2 + |H_{z1}|^2) dx + \int_{-c/2}^{-d/2} (|H_{x2}|^2 + |H_{z2}|^2) dx + \int_{-a/2}^{-c/2} (|H_{x3}|^2 + |H_{z3}|^2) dx \right] + R_s \cdot \int_0^b |H_{z3}(x = -a/2)|^2 dy$$

is the power loss in the metallic walls;

$$P_d = (\omega \epsilon_0 \epsilon_{r1} \tan \delta) \cdot \left( \int_0^b \int_{-d/2}^0 |E_{y1}|^2 dx dy + \int_0^b \int_{-a/2}^{-c/2} |E_{y3}|^2 dx dy \right)$$

is the power loss in the solid dielectric material inside the waveguide (the air in the region 2 is assumed as lossless dielectric);

$$P_{10} = [\beta_{10}/(\omega \mu_0)] \cdot \int_0^b \left[ \int_{-d/2}^0 |E_{y1}|^2 dx + \int_{-c/2}^{-d/2} |E_{y2}|^2 dx + \int_{-a/2}^{-c/2} |E_{y3}|^2 dx \right] dy$$

is the power flowing down the PDF-RW;  $R_s = \sqrt{\omega \mu_0 / (2\sigma_m)}$  is the surface resistance of the metallic walls;  $\sigma_m$  is the conductivity of the metallic walls;  $\tan \delta$  is the loss tangent of the solid dielectric inside the waveguide, while  $H_{xi} = -\beta_{10}/(\omega \mu_0) \cdot E_{yi}$ ,  $E_{yi}$  are given by Eq. (3b);  $H_{zi}$  is given by Eqs. (2) and (4a)–(4c),  $i = 1, 2$ , and 3.

If the expressions for the normalized constants  $A_2/B_1$ ,  $B_2/B_1$  and  $A_3/B_1$  are found (see Appendix B), then, the expressions for  $P_{10}$ ,  $P_l$ , and  $P_d$  normalized to  $B_1^2$  may be written. In this way,  $\alpha_c$  and  $\alpha_d$  values may be computed.

Numerical results obtained for  $\alpha_c$  and  $\alpha_d$  by using the formulas given above, versus the HFSS results are presented graphically in Fig. 6, for different ratios of  $c/a$  and  $d/a$ , where  $a = 20$  mm,  $b = 1.5$  mm,  $\epsilon_{r1} = 4.4$ ,  $\epsilon_{r2} = 1$ ,  $\sigma_m = 5.8 \cdot 10^7$  S/m (copper), and  $\tan \delta = 0.02$ . Because the air inside the waveguide is assumed lossless, the attenuation due to the dielectric losses for the air-filled homogeneous RW ( $c = a$  and  $d = 0$ ) is equal to zero.

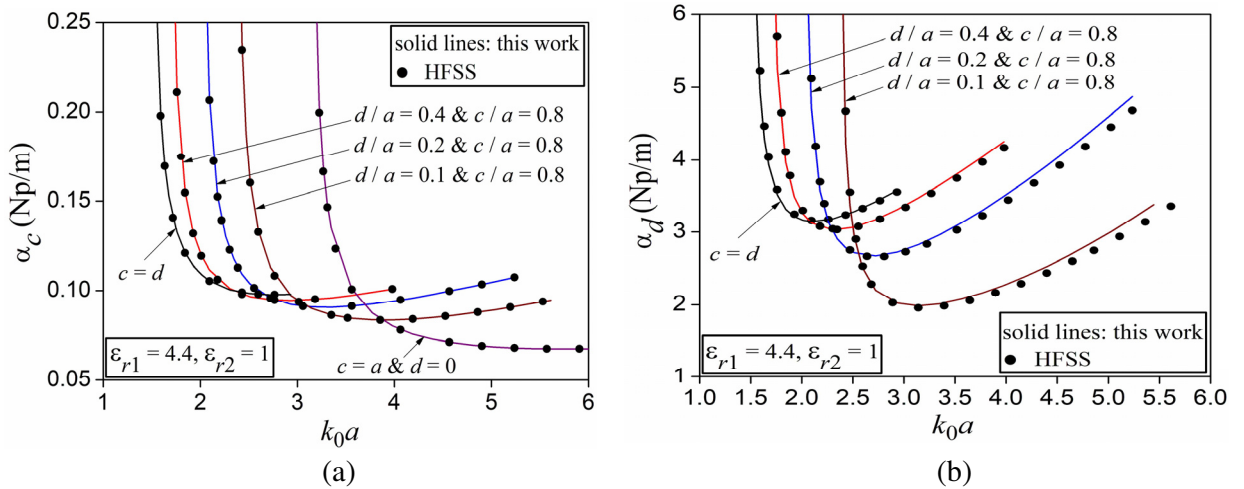


**Figure 6.**  $TE_{10}$  attenuation constant of the PDF-RW, due to (a) the conductor losses and (b) the dielectric losses, versus the normalized propagation constant in the free space  $k_0a$ , for different ratios of  $c/a$  and  $d/a$  ( $a = 20$  mm,  $b = 1.5$  mm,  $\epsilon_{r1} = 4.4$ ,  $\epsilon_{r2} = 1$ ,  $\sigma_m = 5.8 \cdot 10^7$  S/m and  $\tan \delta = 0.02$ ).

As shown in Fig. 6,  $\alpha_c$  and  $\alpha_d$  values are very high for frequencies close to the  $TE_{10}$  cutoff frequencies, but these values decrease rapidly as the frequency increases. Also,  $\alpha_c$  and  $\alpha_d$  curves show that depending on the PDW-RW geometric dimensions, different minimum values at different frequency values may be obtained. It is also observed that the minimum values of  $\alpha_c$  are much closer to each other than the situation observed for  $\alpha_d$ . As the frequency increases above the values for which the attenuation constants reach the minimum values,  $\alpha_c$  increases much slowly compared to  $\alpha_d$ , for the same  $d/a$  ratios. The highest values for the attenuation constants  $\alpha_c$  and  $\alpha_d$  are obtained for the homogeneous RW with  $c = d$ .

The overall attenuation constant decreases as the ratio  $d/a$  decreases. However, as shown in Fig. 3, the ratio  $f_{c-TE20}/f_{c-TE10}$  may have small values when  $d/a$  is very small. In design, the cross section geometric dimensions (see Fig. 1) may be optimized such as to balance the waveguide frequency bandwidth and insertion losses.

#### 4. CONCLUSIONS

Equations for the  $TE_{m0}$  propagation constants and cutoff frequencies have been developed for a more general PDF-RW cross section configuration than other configurations reported up to now. By changing the geometric dimensions of the PDF-RW analyzed in this paper, new PDF-RW configurations may be investigated and particular cases also reported by other authors. Based on these equations, broadband SIWs with low insertion losses may be designed. The equations developed in this paper have been solved using the Mathcad software. The results presented in this paper have been validated comparing them with the results obtained by using HFSS.

#### APPENDIX A.

Using Eqs. (3b) and (4a), (4b), the boundary condition  $E_{y1} = E_{y2}$  at  $x = -d/2$  leads to:

$$\frac{k_{c2}}{k_{c1}} = \frac{B_2}{B_1} \cdot \frac{\cos\left(k_{c2}\frac{d}{2}\right)}{\cos\left(k_{c1}\frac{d}{2}\right)} \cdot \left[ \frac{A_2}{B_2} \tan\left(k_{c2}\frac{d}{2}\right) + 1 \right], \quad \text{for } m \text{ odd} \quad (\text{A1a})$$

and

$$\frac{k_{c2}}{k_{c1}} = \frac{B_2}{A_1} \cdot \frac{\cos\left(k_{c2}\frac{d}{2}\right)}{\sin\left(k_{c1}\frac{d}{2}\right)} \cdot \left[ \frac{A_2}{B_2} \tan\left(k_{c2}\frac{d}{2}\right) + 1 \right], \quad \text{for } m \text{ even.} \quad (\text{A1b})$$

Imposing the condition  $H_{z1} = H_{z2}$  at  $x = -d/2$  and using Eqs. (4a) and (4b), the following relations are obtained:

$$\frac{B_1}{B_2} = -\frac{\cos\left(k_{c2}\frac{d}{2}\right)}{\sin\left(k_{c1}\frac{d}{2}\right)} \cdot \left[ \frac{A_2}{B_2} - \tan\left(k_{c2}\frac{d}{2}\right) \right], \quad \text{for } m \text{ odd,} \quad (\text{A2a})$$

and

$$\frac{A_1}{B_2} = \frac{\cos\left(k_{c2}\frac{d}{2}\right)}{\cos\left(k_{c1}\frac{d}{2}\right)} \cdot \left[ \frac{A_2}{B_2} - \tan\left(k_{c2}\frac{d}{2}\right) \right], \quad \text{for } m \text{ even.} \quad (\text{A2b})$$

Combining Eqs. (A1a), (A2a) and then (A1b), (A2b):

$$\frac{A_2}{B_2} = \frac{\tan\left(k_{c2}\frac{d}{2}\right) - \frac{k_{c1}}{k_{c2}} \cdot \tan\left(k_{c1}\frac{d}{2}\right)}{1 + \frac{k_{c1}}{k_{c2}} \cdot \tan\left(k_{c1}\frac{d}{2}\right) \cdot \tan\left(k_{c2}\frac{d}{2}\right)}, \quad \text{for } m \text{ odd} \quad (\text{A3a})$$

and

$$\frac{A_2}{B_2} = \frac{\frac{k_{c1}}{k_{c2}} + \tan\left(k_{c1}\frac{d}{2}\right) \cdot \tan\left(k_{c2}\frac{d}{2}\right)}{\tan\left(k_{c1}\frac{d}{2}\right) - \frac{k_{c1}}{k_{c2}} \cdot \tan\left(k_{c2}\frac{d}{2}\right)}, \quad \text{for } m \text{ even.} \quad (\text{A3b})$$

Imposing  $E_{y3} = E_{y2}$  at  $x = -c/2$  and  $H_{z3} = H_{z2}$  at  $x = -c/2$ , using Eqs. (3b) and (4b), (4c), the following expressions are obtained for any  $m$ :

$$\frac{k_{c2}}{k_{c1}} = -\frac{B_2}{A_3} \cdot \frac{\cos\left(k_{c2}\frac{c}{2}\right)}{\sin\left(k_{c1}\frac{a-c}{2}\right)} \cdot \left[ \frac{A_2}{B_2} \tan\left(k_{c2}\frac{c}{2}\right) + 1 \right], \quad (\text{A4a})$$

and

$$\frac{A_3}{B_2} = \frac{\cos\left(k_{c2}\frac{c}{2}\right)}{\cos\left(k_{c1}\frac{a-c}{2}\right)} \cdot \left[ \frac{A_2}{B_2} - \tan\left(k_{c2}\frac{c}{2}\right) \right], \quad (\text{A4b})$$

Also, combining Eqs. (A4a) and (A4b):

$$\frac{k_{c2}}{k_{c1}} = -\frac{1}{\tan\left(k_{c1}\frac{a-c}{2}\right)} \cdot \frac{\frac{A_2}{B_2} \tan\left(k_{c2}\frac{c}{2}\right) + 1}{\frac{A_2}{B_2} - \tan\left(k_{c2}\frac{c}{2}\right)}, \quad \text{for any } m, \text{ odd or even.} \quad (\text{A5})$$

If the expression of  $A_2/B_2$  given by Eq. (A3a) is used in Eq. (A5), Equation (5a) is obtained. Also, using  $A_2/B_2$  given by Eq. (A3b) in Eq. (A5), Equation (5b) is obtained.

## APPENDIX B.

The expressions for the normalized constants  $A_2/B_1$ ,  $B_2/B_1$ , and  $A_3/B_1$  for  $TE_{m0}$  with  $m$  odd may be obtained as follows.

Using  $A_2/B_2$  given by Eq. (A3a) in Eq. (A1a) or (A2a),  $B_2/B_1$  may be derived. Knowing  $A_2/B_2$  and  $B_2/B_1$ , then  $A_2/B_1 = (A_2/B_2) \cdot (B_2/B_1)$ . Also, using Eq. (A3a) in Eq. (A4a) or (A4b),  $A_3/B_2$  may be obtained. Knowing  $A_3/B_2$  and  $B_2/B_1$ , then  $A_3/B_1 = (A_3/B_2) \cdot (B_2/B_1)$ .

Note that the expressions for all these normalized constants depend on  $k_{c1}$  and  $k_{c2}$ , which may be computed with Eq. (1), if  $\beta_{10}$  is obtained firstly as shown in Section 2.

## REFERENCES

1. Uchimura, H., T. Takenoshita, and M. Fujii, "Development of a laminated waveguide," *IEEE MTT-S International Microwave Symposium Digest*, Vol. 3, 1811–1814, 1998.
2. Deslandes, D. and K. Wu, "Integrated microstrip and rectangular waveguide in planar form," *IEEE Microwave and Wireless Components Letters*, Vol. 11, No. 2, 68–70, 2001.
3. Wu, K., D. Deslandes, and Y. Cassivi, "The substrate integrated circuits — A new concept for high-frequency electronics and optoelectronics," *Telecommunications in Modern Satellite, Cable and Broadcasting Service*, Vol. 1, 2003.

4. Cassivi, Y. and K. Wu, "Substrate integrated nonradiative dielectric waveguide," *IEEE Microwave and Wireless Components Letters*, Vol. 14, No. 3, 89–91, 2004.
5. Bozzi, M., M. Pasian, and L. Perregrini, "Modeling of losses in substrate integrated waveguide components," *International Conference on Numerical Electromagnetic Modeling and Optimization for RF, Microwave, and Terahertz Applications (NEMO)*, Pavia, Italy, May 2014.
6. Deslandes, D. and K. Wu, "Design considerations and performance analysis of substrate integrated waveguide components," *Proc. of European Microwave Conference*, 881–884, Milano, Sep. 2002.
7. Xu, F. and K. Wu, "Guided-wave and leakage characteristics of substrate integrated waveguide," *IEEE Transactions on Microwave Theory and Techniques*, Vol. 53, No. 1, 66–73, 2005.
8. Ranjkesh, N. and M. Shahabadi, "Reduction of dielectric losses in substrate integrated waveguide," *Electronics Letters*, Vol. 42, No. 21, 1230–1231, 2006.
9. Jin, L., R. Lee, and I. Robertson, "Analysis and design of a novel low-loss hollow substrate integrated waveguide," *IEEE Transactions on Microwave Theory and Techniques*, Vol. 62, No. 8, 1616–1624, 2014.
10. Belenguer, A., H. Esteban, A. L. Borja, and V. E. Boria, "Empty SIW technologies: A major step toward realizing low-cost and low-loss microwave circuits," *IEEE Microwave Magazine*, Vol. 20, No. 3, 24–45, 2019.
11. Pozar, D. M., *Microwave Engineering*, 4th Edition, John Wiley & Sons, 2012.
12. Collin, R. E., *Foundations for Microwave Engineering*, 2nd Edition, John Wiley & Sons, 2001.
13. Ayres, W. P., P. H. Vartanian, and A. L. Helgesson, "Propagation in dielectric slab loaded rectangular waveguide," *IRE Transactions on Microwave Theory and Techniques*, Vol. 6, No. 2, 215–222, 1958.
14. Deslandes, D., M. Bozzi, P. Arcioni, and K. Wu, "Substrate integrated slab waveguide (SISW) for wideband microwave applications," *Proc. IEEE Microwave Theory and Techniques Society Int. Microwave Symp. Dig.*, Vol. 2, 1103–1106, 2003.
15. Khanjar, K. A. and T. Djerafi, "Partially dielectric-filled empty substrate integrated waveguide design for millimeter-wave applications," *Progress In Electromagnetics Research C*, Vol. 87, 135–146, 2018.
16. Gardiol, F. E., "Higher-order modes in dielectrically loaded rectangular waveguides," *IEEE Transactions on Microwave Theory and Techniques*, Vol. 16, No. 11, 919–924, 1968.
17. Bigelli, F., D. Mencarelli, M. Farina, G. Venanzoni, P. Scalmati, C. Renghini, and A. Morini, "Design and fabrication of a dielectricless substrate-integrated waveguide," *IEEE Transactions on Components, Packaging and Manufacturing Technology*, Vol. 6, No. 2, 256–261, 2016.
18. Belenguer, A., H. Esteban, and V. E. Boria, "Novel empty substrate integrated waveguide for high-performance microwave integrated circuits," *IEEE Transactions on Microwave Theory and Techniques*, Vol. 62, No. 4, 832–839, 2014.
19. Parment, F., A. Ghiotto, T. P. Vuong, J. M. Duchamp, and K. Wu, "Air-filled substrate integrated waveguide for low-loss and high power-handling millimeter-wave substrate integrated circuits," *IEEE Transactions on Microwave Theory and Techniques*, Vol. 63, No. 4, 1228–1238, 2015.
20. *High Frequency Structure Simulator (HFSS) — User's Guide* (Ansoft Corporation).